JGR Solid Earth

RESEARCH ARTICLE
10.1029/2020JB019854

The Lithospheric Structure of the Gibraltar Arc System From Wide-Angle Seismic Data

Laura Gómez de la Peña[1], Ingo Grevemeyer[1], Heidrun Kopp[1,2], Jordi Díaz[3], Josep Gallart[3], Guillermo Booth-Rea[4], Eulàlia Gràcia[5], and César R. Ranero[5,6]

[1]GEOMAR Helmholtz Centre for Ocean Research Kiel, Kiel, Germany, [2]Department of Geosciences, Christian-Albrechts-Universität zu Kiel, Kiel, Germany, [3]Institute of Earth Sciences Jaume Almera, CSIC, Barcelona, Spain, [4]Instituto Andaluz de Ciencias de la Tierra, UGR-CSIC, Granada, Spain, [5]Barcelona Center for Subsurface Imaging, Institut de Ciències del Mar, CSIC, Barcelona, Spain, [6]ICREA, Barcelona, Spain

Abstract In continental settings, seismic failure is generally restricted to crustal depth. Crustal structure is therefore an important proxy to evaluate seismic hazard of continental fault systems. Here we present a seismic velocity model across the Gibraltar Arc System, from the Eurasian Betics Range (South Iberian margin), across offshore East Alboran and Pytheas (African margin) basins, and ending onshore in North Morocco. Our results reveal the nature and configuration of the crust supporting the coexistence of three different crustal domains: the continental crust of the Betics, the continental crust of the Pytheas Basin (south Alboran Basin) and onshore Morocco, and a distinct domain formed of magmatic arc crust under the East Alboran Basin. The magmatic arc under the East Alboran Basin is characterized by a velocity structure containing a relatively high-velocity lower crust (~7 km/s) bounded at the top and base by reflections. The lateral extension of this crust is mapped integrating a second perpendicular wide-angle seismic profile along the Eastern Alboran basin, together with basement samples, multibeam bathymetry, and a grid of deep-penetrating multichannel seismic profiles. The transition between crustal domains is currently unrelated to extensional and magmatic processes that formed the basin. The abrupt transition zones between the different crustal domains support that they are bounded by crustal-scale active fault systems that reactivate inherited structures. Seismicity in the area is constrained to upper-middle crust depths, and most earthquakes nucleate outside of the magmatic arc domain.

Key Points:
- New velocity model reveals the lithospheric structure under the Betics (South Iberia), the Alboran Basin, and the North African margin
- The East Alboran Basin is floored by magmatic arc crust, while the southern area of the Alboran Basin is floored by continental crust
- Seismic activity is constrained to the upper-middle continental crust; crustal domains are likely bounded by active faults

Supporting Information:
- Supporting Information S1

Correspondence to:
L. Gómez de la Peña,
lgomez@geomar.de

Citation:
Gómez de la Peña, L., Grevemeyer, I., Kopp, H., Díaz, J., Gallart, J., Booth-Rea, G., et al. (2020). The lithospheric structure of the Gibraltar Arc System from wide-angle seismic data. *Journal of Geophysical Research: Solid Earth*, *125*, e2020JB019854. https://doi.org/10.1029/2020JB019854

Received 25 MAR 2020
Accepted 6 AUG 2020
Accepted article online 13 AUG 2020

1. Introduction

The westernmost Mediterranean is a seismically active zone, controlled by the convergence of the European and African plates at a rate of 4.5 mm/year (McClusky et al., 2003; Stich et al., 2006). Offshore large earthquakes have been recently recorded by the permanent onshore network (i.e., Al-Idrissi, M_w 6.4, 2016) (Gràcia et al., 2019). Historical earthquakes with intensities between VIII and X (Palano et al., 2015; Peláez et al., 2007; Perea et al., 2012) are also described, as well as tsunamis (Maramai et al., 2014) in the coastal areas. Due to the low plate convergence velocity, these large earthquakes have long recurrence periods, as supported by onshore surveys (>1,000 years, Gràcia et al., 2006). Local deployment of offshore stations provides evidence for active faulting, recording earthquakes with magnitudes <3.8 M_w (Grevemeyer et al., 2015). Previous studies suggested that the location of main faults in the area is controlled by crustal structure (Gómez de la Peña et al., 2018; Gràcia et al., 2019) and that seismicity is constrained to crustal depths (Grevemeyer et al., 2015). Thus, understanding the deep structure of this region is fundamental to understand the seismicity distribution and to assess its seismogenic potential.

The general framework of the western Mediterranean upper mantle is provided by regional tomography models (Spakman et al., 2018; Spakman & Wortel, 2004), but higher-resolution models defining crustal structure are lacking. These models are of great importance to study the formation and tectonic processes at regional scale. We focus our study in the Gibraltar Arc System, the westernmost Mediterranean Arc. The Gibraltar Arc System is formed by the Betics and the Rif orogenic belts onshore with the offshore Alboran Basin located in between and the Gulf of Cadiz to the west (Figure 1a), containing basement-involved deformation structures and a Neogene accretionary prism at the front of the subduction (Rovere et al., 2004; Zitellini et al., 2009). The detailed nature of the crustal and upper mantle structure in this

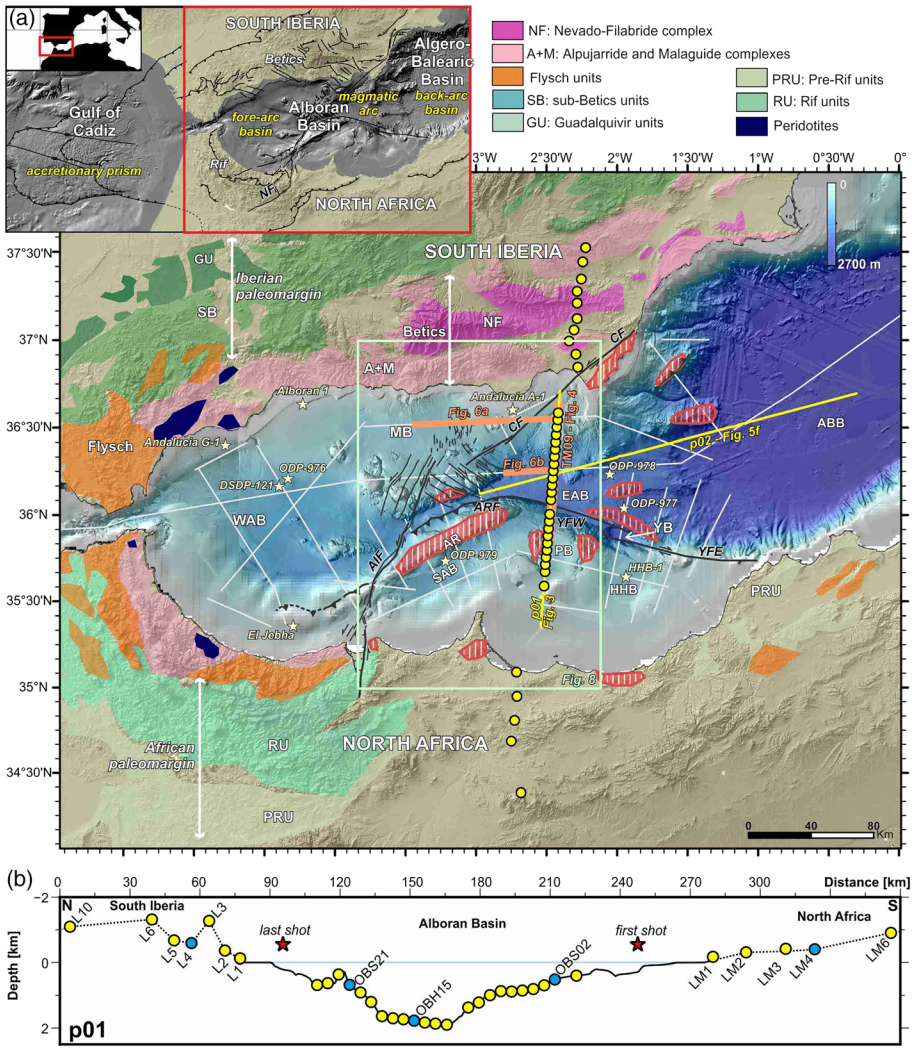

Figure 1. Topographic and bathymetric map of the Alboran Basin region (multibeam bathymetry—Ballesteros et al., 2008; Gómez de la Peña et al., 2016; Gràcia et al., 2012, 2019—completed with SRTM and GEBCO compilations). Onshore, the main tectonic domains are shown (see color legend, Mancilla et al., 2015). Offshore, the location of the main subbasins and tectonic features is displayed. Volcanic outcrops onshore and dredged/drilled volcanic highs offshore from Middle Miocene to Lower Pliocene age are shown (red polygons, Duggen et al., 2008). The location of the two WAS profiles shown in this work is depicted, as well as the location of the OBS/OBH and onshore stations for Profile p01 (yellow circles), TOPOMED MCS profiles (gray lines), and wells (light yellow stars). Inset: Location of the study area and general view of the Gibraltar Arc System. The red rectangle delineates the area shown in the main figure. ABB, Algero-Balearic Basin; AIF, Al-Idrissi Fault; AR, Alboran Ridge; ARF, Alboran Ridge Fault; CF, Carboneras Fault; EAB, East Alboran Basin; HBB, Habibas Basin; MB, Malaga Basin; NF, Nekor Fault; PB, Pytheas Basin; SAB, South Alboran Basin; WAB, West Alboran Basin; YB, Yusuf Basin; YFW, Yusuf Fault West segment; YFE, Yusuf Fault East segment. (b) Topography/bathymetry along the p01 profile. Stations shown in Figure 2 are colored in blue.

area has remained unresolved due to the lack of seismic refraction data covering the offshore part of the system, the Alboran Basin.

Onshore, the Moho topography and crustal thickness variations are mapped by passive seismology methods (Mancilla et al., 2015; Mancilla & Diaz, 2015). Recent tomographic models focusing on Iberia and North Africa provided more detailed tomographic images of the mantle (e.g., Bezada et al., 2013; Bonnin et al., 2014; Villaseñor et al., 2015). These models support that the Moho under the Alboran Basin ranges between ~13 and ~27 km (e.g., Díaz et al., 2016). However, the lack of offshore seismic stations resulted in a poorly resolved model in this area (Mancilla & Diaz, 2015; Palomeras et al., 2017), producing a coarse characterization of the crust/mantle variations under the Alboran Basin. The offshore crustal configuration has been

studied using multichannel seismic (MCS) data (Gómez de la Peña et al., 2018) and a temporal deployment of an ocean-bottom-seismometer network for a passive microseismicity survey (Grevemeyer et al., 2015). Although both methods indicate remarkable thickness variations (up to ~4 s two-way travel time [TWTT]) and different types of crust under the Alboran Basin, wide-angle seismic (WAS) data are a prerequisite for precise information on the seismic velocity-depth distribution to unambiguously constrain the nature of the crust and upper mantle.

Active-source WAS surveys on the area are scarce and currently not sufficient to provide a comprehensive image of the crust. Onshore Morocco, an active-source WAS survey of the Rif area (RIFSIS project, Gil et al., 2014) has found the Moho >40 km depth under the Rif (western Morocco, inset Figure 1) that shoals to ~28 km east of the Nekor Fault (eastern Morocco, inset Figure 1). Onshore South Iberia, the Moho is located between 30 and 40 km depths below the Betics and shoals toward the coastline (Banda et al., 1993). A narrow area across the South Iberian onshore-offshore transition was surveyed by the ESCI project (Gallart et al., 1995), finding a different Moho wide-angle reflection under the Alboran Basin (~6–8 TWTT) and under the Betics (~11 s TWTT). Offshore, a first attempt to map crustal thickness was carried out by the Working Group Deep Seismic Sounding Alboran 1974 (1978), delineating the Moho at ~18 km depth under the Alboran Basin. Only the transition between the East Alboran Basin (EAB) and the Algero-Balearic Basin has been surveyed with WAS data (Booth-Rea et al., 2018), supporting the presence of magmatic crust under the easternmost Alboran Basin and oceanic crust under the Algero-Balearic Basin. However, the occurrence of this crust should be further constrained. Moreover, the presence of magmatic arc crust under the Alboran Basin is not generally accepted, and some models propose thinned continental crust flooring the basin (e.g., Comas et al., 1999; Medaouri et al., 2014).

Here we present results of a 2-D transect with modern WAS and coincident MCS data oriented approximately N-S across the Alboran Basin (Figures 1a and 1b). The interpretation of the transect is complemented with results from a crossing WAS line running roughly W-E (Figure 1a; Booth-Rea et al., 2018) and several crustal-scale crossing MCS lines (Figure 1a; Gómez de la Peña et al., 2018). The WAS profiles characterize the offshore and onshore domains of the Gibraltar Arc System and integrated with the MCS images, and seismicity data provide a comprehensive characterization of the lithospheric and tectonic structure under the Alboran Basin and its margins. The main objectives of this study are (1) to present the *P* wave velocity structure under the eastern Gibraltar Arc System, (2) to compare the *Vp* model to the coincident seismic image and interpret the results in terms of the distribution of geological domains, and (3) to discuss the implications of the crustal structure for earthquakes nucleation and seismicity.

2. Geologic Setting

Plate convergence and subduction-related orogenic processes controlled the evolution of the Mediterranean arcs during the Late Cenozoic (Royden & Faccenna, 2018). The emergence and formation of the subduction systems shaped the current geologic domains and crustal structure of the area, which in the case of the Gibraltar Arc System is still poorly understood. The formation of the Gibraltar Arc System began in the Late Oligocene. The Miocene westward migration of the subduction system led to the collision of the allochthonous Alboran terrane with the Tethyan South-Iberian and African margins (Platt et al., 2013; Van Hinsberger et al., 2014). This terrane is stacked over the Iberia and Africa passive margins, forming the inner zones of the Betics and the Rif ranges (Figure 1a). At the same time, extensional processes took place within the Alboran Basin (e.g., Comas & Soto, 1999; Watts et al., 1993). Different hypotheses have been invoked to explain the extension: convective removal (Dewey et al., 1989; Platt & Vissers, 1989), mantle delamination (García-Dueñas et al., 1992; Seber et al., 1996), and subduction models (Blanco & Spakman, 1993; Royden, 1993). However, tomographic imaging of a slab hanging below the Gibraltar Arc System supports the relation of the Gibraltar Arc with a subduction system (García-Castellanos & Villaseñor, 2011; Wortel & Spakman, 2000). In this context, slab roll-back and lithospheric tearing at the edges of the subduction system are the most plausible mechanisms for the extension (e.g., Chertova et al., 2014; Faccenna et al., 2014). In conjunction with the subduction system, volcanic activity occurred in the basin. Three different episodes have been described: (1) tholeiitic dykes found only onshore (Late Oligocene-Early Miocene, Marchesi et al., 2012; Torres-Roldan et al., 1986), (2) calk-akaline and tholeiitic volcanism in the central and eastern part of the Alboran Basin, related to subduction fluids coeval to Si-K rich shoshonitic magmatism onshore

(Duggen et al., 2008), and (3) alkaline volcanism at the basin margins that supports the influx of asthenospheric material (Messinian to Quaternary, Duggen et al., 2004, 2008). Based on the volcanic rock distribution and the internal structure of the crust observed in seismic images, some studies proposed thinned continental crust affected locally by magmatism under the EAB (Comas et al., 1999; Medaouri et al., 2014), while others proposed magmatic arc crust (Booth-Rea et al., 2007, 2018; Duggen et al., 2005, 2008; Gómez de la Peña et al., 2018).

Onshore, the Betics and Rif orogenic belts consist of four tectonic domains (Figure 1): (1) the foreland basins, comprising Neogene and Quaternary sediments; (2) the external zones, a fold-and-thrust belt composed by Mesozoic to Cenozoic sediments (Crespo-Blanc & Frizon de Lamotte, 2006; Gràcia et al., 2003; Sanz De Galdeano, 1990); (3) the Flysh units, representing the oceanic sedimentary cover of the Tethys domain (Luján et al., 2006); and (4) the internal complexes, a stack of three polymetamorphic domains—two allochtonous terranes coming from the Alboran Domain (i.e., the Alpujarride/Sebtide and the Malaguide/Ghomaride complexes, in the Betics and the Rif, respectively) (García-Dueñas et al., 1992; Michard et al., 2008; Sanz De Galdeano, 1990) and a third terrane, the Nevado Filabride in the Betics, which likely was part of the subducted South Iberian margin (Booth-Rea et al., 2015; Platt et al., 2005).

During the Messinian, between 6 and 7 Ma, subduction terminated or highly decreased its activity (Iribarren et al., 2007), leading to a new geodynamic scenario. Extensional processes ended offshore, and the area is now undergoing shortening due to the European and African plates converging NW-SE (~4.5 mm/year, McClusky et al., 2003), resulting in the tectonic inversion of several fault systems in the area (Giaconia et al., 2015; Martínez-García et al., 2013). The most prominent faults in the Alboran Basin are the Carboneras, Yusuf, Al-Idrissi, and Alboran Ridge fault systems (Figure 1a).

3. Data and Methods

3.1. Data Acquisition and Phase Interpretation

The WAS data were acquired during the WESTMED project (Cruise M69/2, August–September 2006) onboard the German RV "*Meteor*". Profile 01 (p01) was recorded using 15 onshore stations and 24 offshore stations (ocean-bottom seismometers and hydrophones—OBS/OBH). However, only 12 onshore stations and 23 offshore stations recorded data. The offshore stations spacing was 4.5 km. Shooting was performed offshore along an ~150 km long profile, using two 32-L BOLT air guns, fired every 60 s (~200 m) at a pressure of 140 bar. Including the onshore stations, the total length of the Profile p01 is 360 km. The profile runs coincident with offshore MCS Profile TM09. This profile was acquired during the TOPOMED cruise (October 2011), onboard the Spanish RV "*Sarmiento de Gamboa*" with a 5,100 m long streamer. TM09 MCS profile was first presented in Gómez de la Peña et al. (2018) and will be used to complement the interpretation of our new WAS velocity model.

We identified four refracted phases and three reflected phases on Profile p01 (Figure 2). Refracted and reflected waves could be identified on all record sections (Figure 2), despite the high-level of noise due to the marine traffic (Figure 2a offset >90 km, Figure 2d offset <−90 km). The different phases were identified based on their geometry, their offsets, and an iterative process of comparing observed and calculated travel times prior to the final inversion (see supporting information for details). A picking error has been assigned to each phase based on the signal to noise ratio of the signals (left panels of Figure 2). The first refracted waves are *Ps* waves (total number of arrivals $n = 888$), traveling through the sedimentary cover. *Ps* are observed only on the offshore stations and show apparent velocities <4 km/s (Figures 2c and 2d). The second refracted waves are *Pg* waves, turning within the crust. We divided them into upper crust (*Pg*1, $n = 5{,}669$), arriving between ~5 and ~25 km offset and with an apparent velocity between ~4.5 and 5.75 km/s, and lower crust (*Pg*2, $n = 4{,}158$), arriving at >20 km offset and with apparent velocities ~5.75–6.5 km/s. Finally, we also identified refracted waves traveling through the mantle, arriving at offsets >80 km and showing an ~8 km/s apparent velocity (*Pn*, $n = 883$, Figures 2a and 2e). The uncertainty associated with the picking of upper crustal arrivals is <0.05 s, increasing to 0.06–0.1 s for the lower crust and mantle phases, respectively.

The first reflected wave is from the basement top (*PsP*, $n = 318$). This energy allows reconstructing the sedimentary thickness along the offshore section of the profile (Figures 2c–2e). In addition, two wide-angle reflections were observed. In the central part of the profile, a first wide-angle reflected wave was recorded

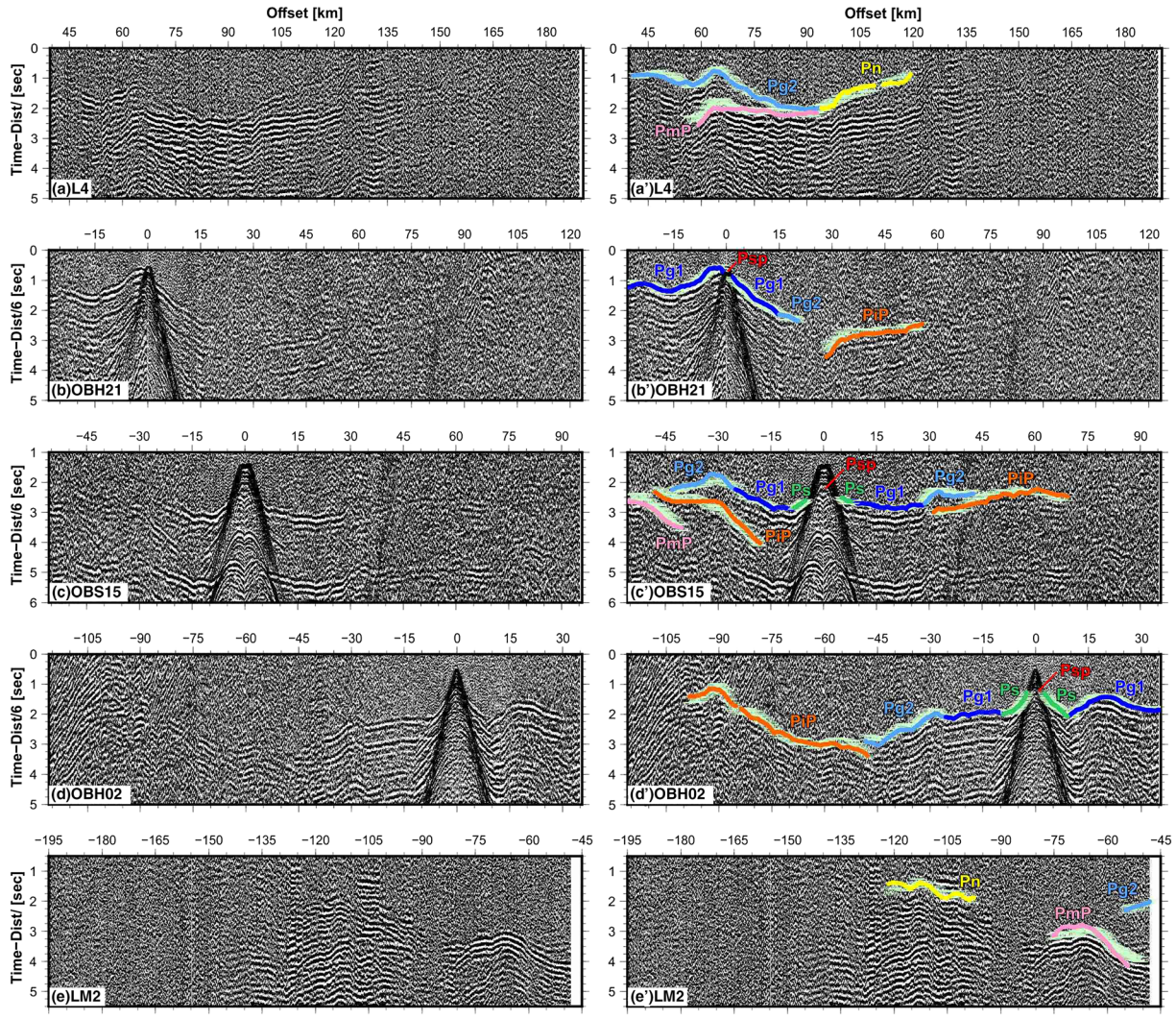

Figure 2. Examples of the recorded sections. Vertical scale is time-reduced by 6 km/s. The identified phases are depicted in the left panels, including the observed travel times (light green lines) and the calculated travel times (colored lines). (a and a′) L4 onshore station recorded section (see also Figure S2a). (b and b′) OBH 21 recorded section. (c and c′) OBS 15 recorded section. (d and d′) OBH 02 recorded section. (e and e′) LM2 onshore station recorded section (see also Figure S2b).

arriving at offsets between ~15 and 50 km (Figures 2b–2d). It corresponds to an intracrustal reflection, labeled *PiP* (n = 4,544). *PiP* was recorded on most OBS/H and at the southernmost stations in Iberia, but neither in North Africa nor on the stations in the Betics (South Iberian margin, Figures 1, 2, and S1b). A second reflection, corresponding to the Moho reflection (*PmP*, n = 1,465), was identified arriving at offsets >40 km (Figure 2). *PmP* is best sampled on the seismic stations in South Iberia and North Africa and just three branches occur on three OBS/H, sampling the seismic Moho in the northern domain of the Alboran Sea and under South Iberia and North Africa, while the Moho has not been observed in the vicinity of the Yusuf fault (Figures 1, 2, and S1d). The uncertainty associated with the picking of the wide-angle reflections ranges between 0.08 and 0.1 s.

3.2. Travel Time Tomography and Uncertainty Assessment

In order to obtain the 2-D *P* wave velocity-depth distribution of the crust and upper mantle as well as the geometry of the identified reflections, we simultaneously inverted the refraction and reflection travel times using TOMO2D (Korenaga et al., 2000). The initial velocity model for the inversion is based on the 1-D velocity model obtained from inversion of *P* and *S* wave arrivals of local earthquakes (Grevemeyer et al., 2015; supporting information). The inversion was executed following a layer-stripping strategy, starting from

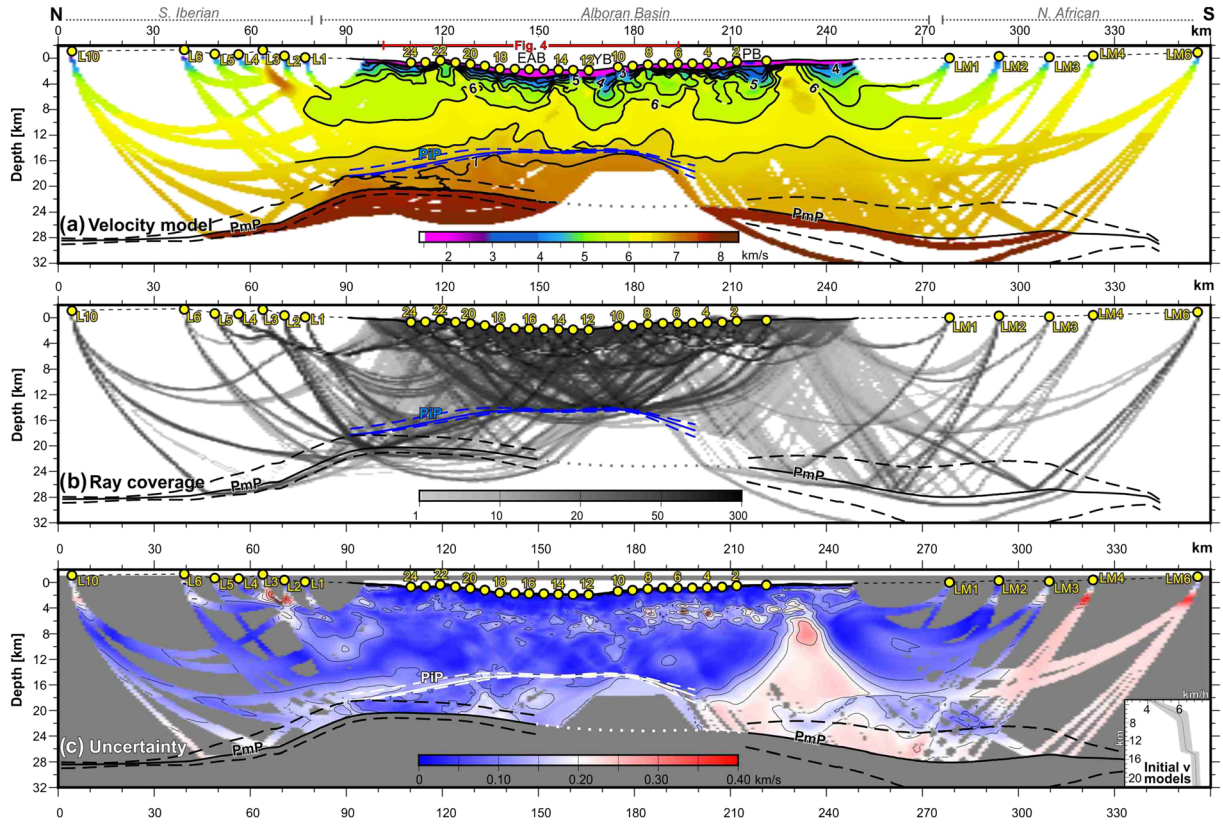

Figure 3. Velocity modeling results. Location of the offshore (Alboran Basin) and onshore parts of the profile is shown at the top of the figure. (a) Final WAS velocity model. This model shows the average result of the Monte Carlo inversions for the crustal velocities and the location of PiP and PmP reflections and includes the mantle velocity. Uncertainty in the reflections depth is shown by the dashed lines. In the areas without PmP reflections, the Moho is shown as a gray dotted line. EAB, East Alboran Basin; PB, Pytheas Basin; YB, Yusuf Basin. (b) Derivative weight sum. This parameter shows an estimation of the rays illuminating an area. (c) Standard deviation in the velocities resulting from the Monte Carlo analysis. The inset shows the Monte Carlo's initial velocity models at km 150.

the shallower layers and progressively updating the deepest ones (Figure S1). This strategy improves the results in the deeper part of the model by avoiding steep changes between consecutive velocity layers, preserving the accuracy in the shallower ones. Only one reflected phase is inverted at a time (Figure S1). We run 10 iterations of the inverse modeling code for *PsP* and five iterations for all the other phases. The final *P* wave velocity model and ray coverage are shown in Figures 3a and 3b.

Uncertainty analysis was tackled through the Monte Carlo approach. This approach also tests the impact of the starting velocity model on the result and provides the standard deviations of the model parameters (velocity and reflector depths, Figure 3c). We excluded the mantle arrivals from the Monte Carlo analysis due to the low number of picks ($n = 883$). We performed 100 inversions with different initial velocity models and compare the results. The initial velocity models for the Monte Carlo analysis were randomly constructed scaling the initial velocity model with a maximum variation of the velocities of 20% (inset of Figure 3c). The results of the Monte Carlo analyses support a root-mean-square (RMS) misfit equal to 0.0934 s (chi-square value, $\chi^2 = 1.858$, Table S2). This analysis documents that the uncertainty is higher in the onshore parts of the profile, while the offshore velocity structure and reflections geometry are well constrained, showing standard deviations <0.10 km/s for the upper-middle crust velocities, <0.15 km/s for the lower crust velocities, <1 km for the *PiP* reflection depth, and <3 km for the *PmP* depth (Figure 3c). The crustal structure shown in Figure 3 is the result of the Monte Carlo analysis, which has been use as input for the *Pn* phase inversion. The mantle velocities are inverted after the Monte Carlo analysis. Uncertainties in the mantle were analyzed using different initial mantle velocities and running a simplified grid search, using the mantle velocity providing the lowest travel time residuals as the appropriate mantle velocity. Due to the limited ray coverage, statistical methods are not possible, and the uncertainty is assessed based on the apparent velocity of the arrivals and the error assigned to the picks. The velocity range considered is the

one that provides a good fit to the apparent velocity within the picking error. Uncertainty is on the order of 0.05 km/s.

4. Results

4.1. Velocity Structure and Reflection Geometry

The mean velocity model and interface positions resulting from the Monte Carlo tomographic inversions are shown in Figure 3a, including the mantle velocities. The results of the Monte Carlo analysis reveal higher uncertainty across the northern and especially the southern extensions of the profile (km 0–90 and km 210–360, respectively, Figure 3c), both in the velocities and in the *PmP* location, due to poor ray coverage (Figure 3b). This is because all shots were fired offshore, causing a lack of crossing rays in the onshore parts of the profile. We distinguish three clearly different crustal configurations along the profile: (1) the South Iberian margin (km 0–90, Figure 3), (2) the EAB (km 90–200, Figure 3), and (3) and the North Africa coastal and continental shelf (containing Pytheas Basin) areas (km 200–360, Figure 3).

4.1.1. The South Iberian Margin

The South Iberian margin is poorly characterized by our data (Figure 3, km 0–90). However, our velocity model does constrain a sediment layer with a moderate velocity (~3–4.5 km/s) between the surface and ~3 km depth, a 4.5–5 km/s upper crust and an apparently homogeneous lower crust characterized by velocities of 6–6.6 km/s. The Moho is located between 28 ± 2 and 23 ± 2 km depths, shallowing toward the Alboran Basin, and it is underlain by mantle velocities of ~7.9 km/s (Figures 3a and S2a).

4.1.2. The EAB

The EAB crust is well illuminated by numerous crossing rays (Figure 3, km 90–200). However, there are no turning or reflected rays from the lower crust in the southern section (Figures 3 and 4a, km 160–200, Figure S1d). Figure 4a shows the offshore portion of the velocity model in the EAB. The EAB is characterized by a complex crust that can be subdivided into four zones: (1) the sedimentary cover, (2) the upper crust, (3) the middle crust, and (4) the lower crust. The sedimentary cover shows a highly variable thickness, from 0 km above basement highs to more than 3 km in local depocenters (e.g., the Yusuf Basin, Figures 3a and 4a, km ~170). It is characterized by <3 km/s velocity in the shallow section and <4.2 km/s in its deeper section. Underneath, the upper crust extends to ~10 km depth, characterized by mean velocities of ~5.4 km/s and a higher velocity gradient than the middle crust. The upper crust grades into the middle crust with velocities ranging between ~6 and ~6.6 km/s. The base of the middle crust is a well-defined boundary between 15 ± 0.1 and 17 ± 1 km producing the *PiP* reflection (Figure 3). This reflection occurs only in the central part of the profile (Figures 2, 3, and S1b) delineating the top of the lower crust. The lower crust thickens from north to south to a maximum of ~7.5 km, with a velocity of ~7 ± 0.1 km/s (Figures 3 and 4a, km 90–200). The Moho reflection (*PmP*) is located at 22 ± 2 km depth (Figures 3 and 4a, km 90–150), deepening toward the south to 28 ± 3 km deep beneath the Moroccan shoreline (Figure 3, km 240–280). The upper mantle is sampled only in the north, with an ~7.9–8 km/s velocity (Figure 3, km 90–150).

4.1.3. North African Coastal and Continental Shelf Area

Under the North African coastal and continental shelf areas, containing the Pytheas Basin (Figure 3, km 200–360), the *PiP* reflection is not observed and the Moho progressively deepens to ~28 ± 3 km depth. The offshore part is characterized by the presence of two sedimentary depocenters (Figure 3, km 200–220 and 235–250), reaching ~4 km of sediment infill. From 4 to 16 km depth, velocities range from ~5.6 to ~6.5 km/s. Here, we cannot distinguish any upper-middle crust velocity structuration because uncertainty of the velocity structure is too high (0.20–0.30 km/s, Figure 3c). The lower crust, between 16 and 28 km, has a velocity of ~6.8 km/s. Mantle arrivals support a mantle velocity of ~8 km/s in this region (Figures 3a and S2b).

4.2. Crustal Reflectivity

The comparison between the *Vp* model and the coincident MCS image (Figures 1 and 4) allows integration between the tectonic structure, crustal reflective fabrics, and *Vp* domains. The MCS profile covers the offshore part of the profile, from the South Iberia shelf across the Pytheas Basin (Figures 1, 3a, and 4). The MCS image (Figure 4c) is compared to the *Vp* model converted from depth to TWTT in Figure 4b.

Based on the crustal reflectivity, the MCS image can be divided into two areas separated by the Yusuf Fault (Figures 1, 4b, and 4c). Below the EAB (Figure 4c, km ~100–170), three layers have been identified in the

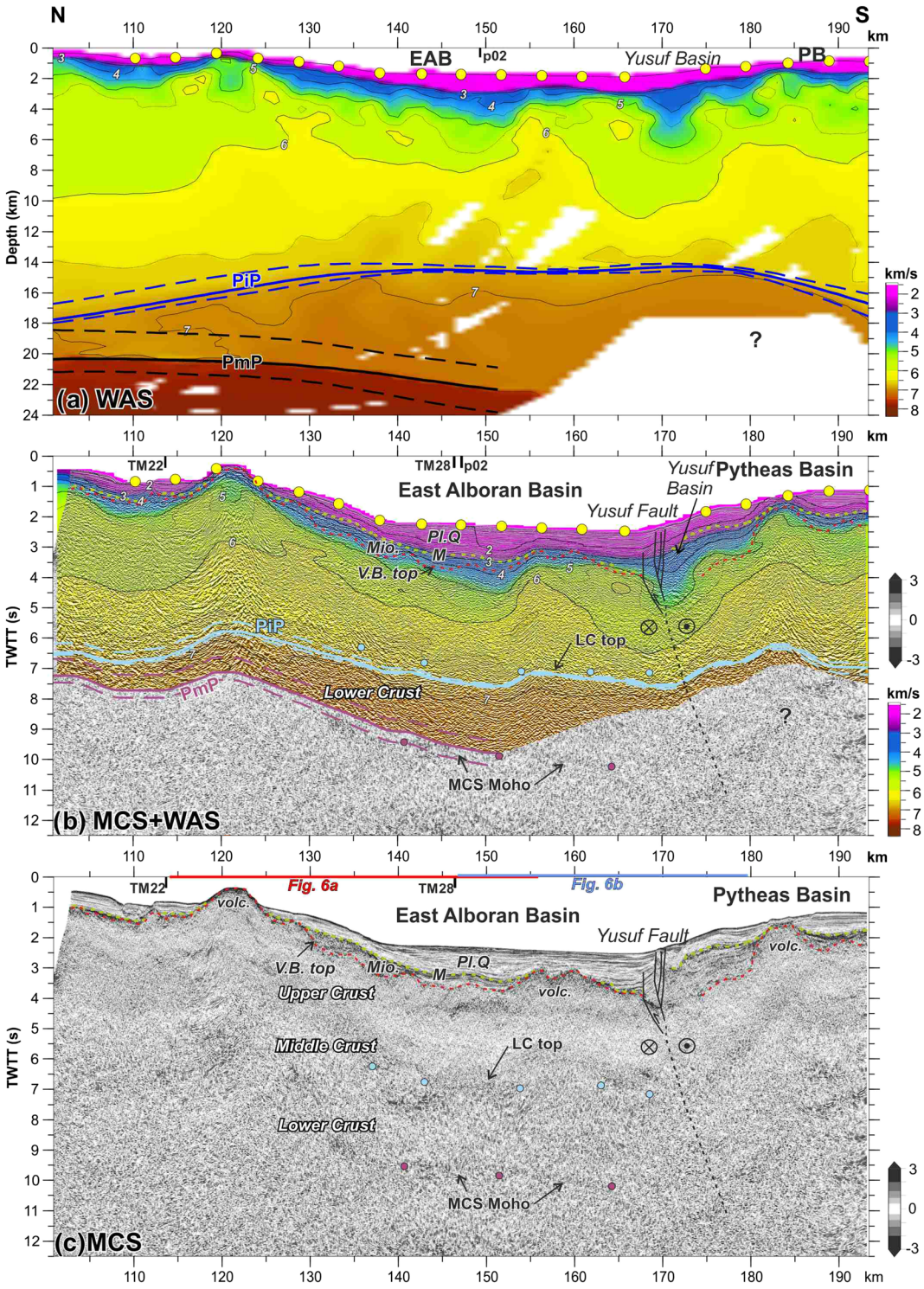

Figure 4. Comparison between the MCS and the WAS profile. (a) Zoomed section of the p01 WAS velocity model, with the vertical axis in depth (km). (b) TM09 MCS profile with the p01 WAS velocity model superposed. Note that the vertical axis is in TWTT (s). Green dashed line marks the *M* reflection, while red dashed line corresponds to the top of the basement. Blue and purple circles correspond, respectively, to the lower crust top and the Moho observed in the MCS. The top of the lower crust inverted from the WAS data (PiP reflection) is represented by a blue line, and the inverted Moho (PmP) by a purple line, including the estimated uncertainty. LC, Lower Crust; M, Messinian top; Mio., Miocene sediments; Pl.Q, Plio-Quaternary sediments; V.B. top, volcanic basement top. (c) TM09 MCS profile. Due to reflectivity changes, it can be divided into the sedimentary cover, upper crust, middle crust, and lower crust. The boundary between the Plio-Quaternary sedimentary units (Pl.Q) and the Miocene units (Mio.) is depicted in green (*M* reflection). The top of the basement is depicted in red. The blue circles delineate the top of the lower crust, while purple circles delineate the Moho reflection. The Yusuf Fault trace is interpreted. VB, volcanic basement; volc., volcanic intrusion/volcano.

basement: (1) a high-reflectivity upper crust with an irregular top that gradually transitions to (2) a low-reflectivity middle crust and (3) a high-reflectivity lower crust characterized by discontinuous parallel reflections (Figure 4c; Booth-Rea et al., 2007; Gómez de la Peña et al., 2018). The Moho is interpreted at the base of the reflective layer. Below the EAB, the Moho is located between 9 and 10 s TWTT (Figures 4b and 4c), while below the North African shelf it is located at ~12 s TWTT (Gómez de la Peña et al., 2018). The top and the base of the high-reflectivity lower crust are in good agreement with the *PiP* and the *PmP* wide-angle reflections (Figure 4b).

5. Discussion

5.1. Crustal Structure

Our transect provides a detailed crustal and upper mantle image of the SE Iberia margin, the EAB, the Pytheas Basin, and the North African margin. This model resolves not only the crustal structure under the Alboran Basin but also its relation to the Spanish and Moroccan continental margins. Further, the *P* wave velocity model provides information on the nature of the basement (Figure 5) and complements the information provided by the MCS images (Figures 4 and 6).

We interpret three different crustal domains: (1) continental crust under the South Iberian margin, (2) magmatic arc crust under the EAB, and (3) continental crust under the North African coastal and continental shelf area, including the Pytheas Basin offshore. The 1-D velocity profiles sampling these areas are displayed in Figure 5, compared to the reference velocity models from data compilations including oceanic (Grevemeyer et al., 2018), continental (Christensen & Mooney, 1995), and magmatic arc (Contreras-Reyes et al., 2011) types of crust (Figure 5b). To provide some 3-D constraints of the crustal configuration, the velocity structure along the E-W Profile p02 (Figure 1; Booth-Rea et al., 2018) is also displayed (Figures 5f and 5g).

5.1.1. Continental Crust Under the South Iberian Margin

The ray coverage under the South Iberian margin is the poorest of the entire profile (Figure 3b). Thus, the velocity model provides a mean velocity value for the crust but the crustal structure, especially below 4 km depth, cannot be resolved in detail. *P* wave velocity values range from 4.5–5 to 6.6 km/s from the upper to the lower crust, supporting a continental nature (Figure 5c). The continental nature is in agreement with the crustal thickness, ~30 km, and the basement samples collected in the near coastal areas (Comas et al., 1999; Jurado & Comas, 1992). Due to the different basement reflectivity, characterized by intracrustal reflections in northern Africa and a more transparent character under the Malaga Basin (Figure 1a; Gómez de la Peña et al., 2018), and the different metamorphism described for the sampled basement rocks in the South Iberian and the North African offshore areas (well location in Figure 7a; Comas et al., 1999; Medaouri et al., 2014), the South Iberian and the North African domains have been interpreted as two different continental domains.

On the SE Iberian record sections, a layered pattern of the energy can be observed (e.g., Figure 2a). However, the only phases that we have been able to identify are *Pg*2, *PmP*, and *Pn* (Figure 2a′). The continuity onshore of the *PiP* reflection has been tested, and our results support that the *PiP* phase is limited to the EAB area (Figure S1b). We identified *PiP* arrivals in L1 and L2 onshore stations (Figure 1b) but not farther away from the coastline. The ray pattern supports that the *PiP* reflection ends under the EAB, at ~90 km (Figures 3 and S1b). Similarly, the correlation of the energy observed onshore with offshore phases has not been possible, excluding the mentioned *Pg*2 and *PmP*. This layered energy pattern has been previously observed in the WAS experiment onshore (Banda et al., 1993) and has been related to the highly heterogeneous crust forming the Betics (i.e., the different stacked terranes and the high lateral variability). These results suggested a different crust under the South Iberian margin and the EAB, consistent with the different thickness and velocities observed in both regions (Figures 5c and 5d).

We identified *Pn* arrivals on the SE Iberian and North African onshore stations (Figures 2a and S2). The inversion of these arrivals provides for the first time a mantle velocity constrained under the Alboran Basin, with values close to ~7.9 km/s (Figures 3a and S2). This result is consistent with regional mantle velocity estimations from earthquake travel times, though somewhat faster than the velocity of 7.8 km/s reported previously (Grevemeyer et al., 2015). However, the approach of Grevemeyer et al. (2015) was a 1-D approximation of the entire Alboran domain that sampled a much larger volume.

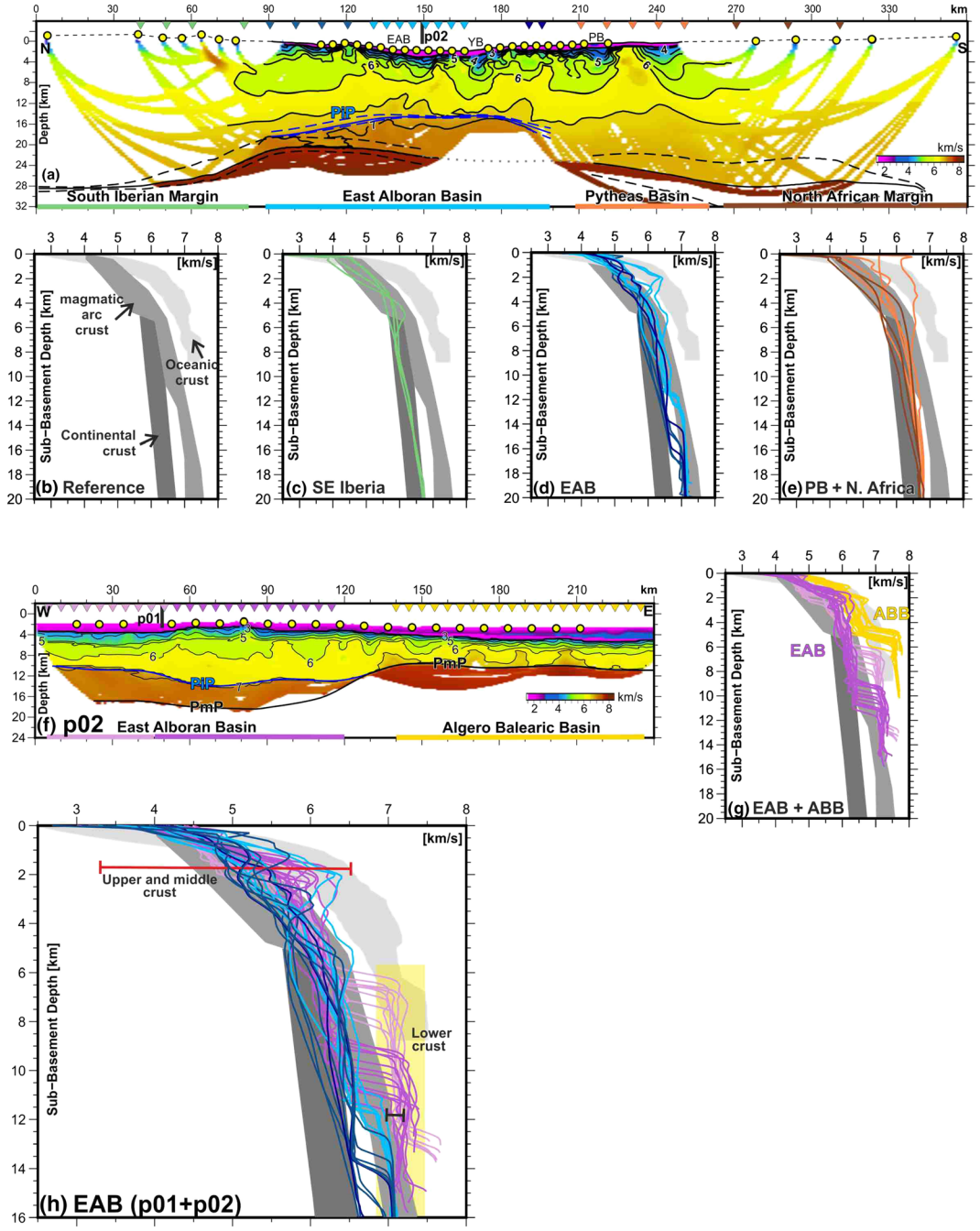

Figure 5. One-dimensional velocity profiles along Profiles p01 and p02. (a) p01 profile. The location of the 1-D velocity profiles displayed in Figures 5c–5e and 5h is shown in the upper part of the image. The color lines in the bottom depict the different areas along the profile. (b) Reference velocity gradients for oceanic (Grevemeyer et al., 2018), magmatic arc (Contreras-Reyes et al., 2011), and continental crust (Christensen & Mooney, 1995). (c) SE Iberian section 1-D velocity profiles. (d) EAB 1-D velocity profiles, divided in the central section (light blue) and its margins (dark blue). (e) Pytheas Basin (PB, orange) and North African section (brown) 1-D velocity profiles. (f) p02 profile (Booth-Rea et al., 2018). Location of the 1-D velocity profiles shown in Figures 5g and 5h is shown in the upper part of the image. (g) EAB (pink colors) and Algero-Balearic Basin (ABB, yellow color) 1-D velocity profiles. (h) Crustal velocities of the EAB, along the N-S p01 profile and the W-E p02 profile.

5.1.2. Magmatic Arc Crust Under the EAB

The crust under the EAB is ~20 km thick, which is much thicker than standard oceanic crust (Christeson et al., 2019; Grevemeyer et al., 2018; White et al., 1992) but thinner than standard continental crust

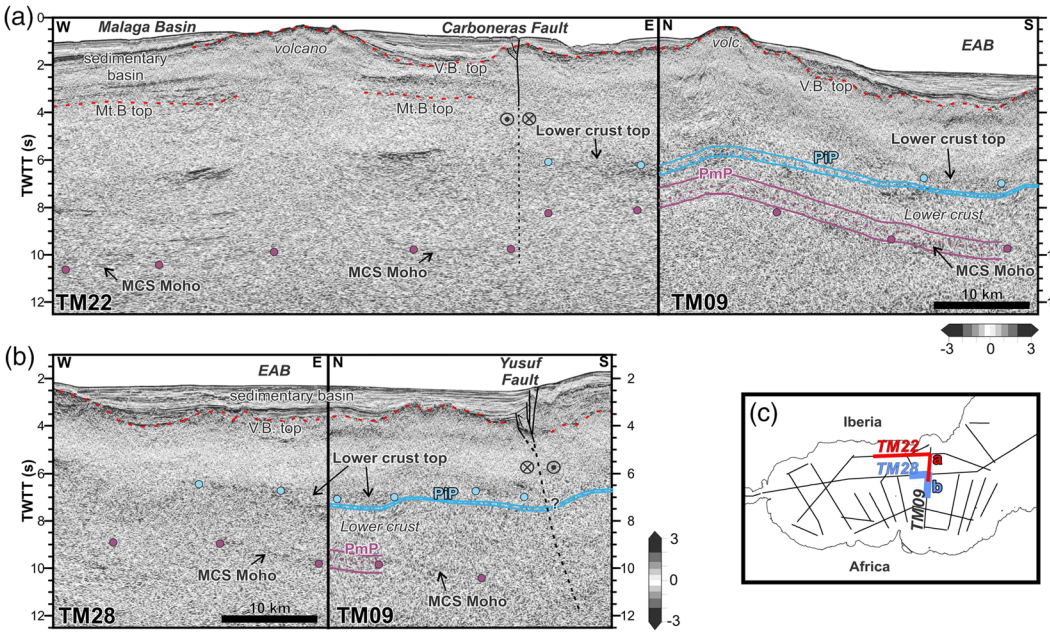

Figure 6. Comparison between N-S MCS section (TM09) and two E-W MCS sections. (a) Combined section of TM22 and TM09 profiles and (b) combined section of TM28 and TM09 profiles. The blue line corresponds with the PiP reflection and the purple line with PmP reflection, including the uncertainty. The blue dots and the purple dots correspond respectively with the top of the lower crust and the Moho reflectivity interpreted in the MCS sections. Compared with the N-S section, a higher reflectivity in the lower crust is observed in the E-W sections, as well as more continuous reflections. V.B., volcanic basement; Mt.B, metamorphic basement; volc., volcanic intrusion/volcano. (c) MCS grid from the TOPOMED cruise and location of the shown profiles.

(Christensen & Mooney, 1995). This crust is characterized by a strong variability in *P* wave velocity in the upper-middle crust (Figures 4a and 5) and a high-velocity lower crust (*Vp* 7 ± 0.1 km/s) bounded by two wide-angle reflections: an intracrustal reflection at its top (*PiP*, Figures 2b–2d, 3, and 4a) and the Moho reflection at its bottom (*PmP*, Figures 2c, 3, and 4a). The lower crust is separated from the upper crust and the middle crust by a large abrupt increase in seismic velocity, of >0.7 km/s (Figures 5d, 5g, and 5h). Velocity in the lower crust is ~7 km/s in the N-S profile (Figures 5a and 5h) and ~7.25 km/s in the W-E profile (p02, Booth-Rea et al., 2018; Figures 5f–5h). The high-velocity lower crust correlates with a layer of high reflectivity making the lower crust of MCS images (Figure 4b). The lateral extension of the high-reflectivity body in MCS images is shown by the W-E profiles, displayed in Figure 6.

Although the crustal velocity structure is variable in magmatic arc settings, a high-velocity lower crust is a common characteristic (Figure 5b; Calvert, 2011; Contreras-Reyes et al., 2011; Shillington et al., 2004). Our observations of the velocity structure and the MCS data, together with the affinity of basement samples as well as the subduction context inferred from tomographic models, agree with a magmatic arc type crust flooring the EAB (Figures 5h and 7) (Booth-Rea et al., 2007, 2018; Duggen et al., 2008; Gómez de la Peña et al., 2018; Hoernle et al., 1999). The 3-D character of the high-velocity lower crust is confirmed by Profile p02 running perpendicular to the Profile p01 presented here (Figures 1 and 5h), showing the same crustal structure under the EAB that transitions to a thinner, oceanic crust toward the Algero-Balearic Basin (Booth-Rea et al., 2018; Figures 5f, 5g, and 7). The interpreted crustal domains are shown in Figure 7.

The middle crust in arc areas has velocities similar to continental crust (e.g., Tatsumi et al., 2008). The EAB upper-middle crust velocities range between 4.2 and 6.6 km/s and thus agree with a relatively high-velocity continental crust (Figure 5h), but the continental crust model cannot explain (1) the crustal thickness, (2) the high-velocity anomalies found in the upper crust (Figures 3 and 4 ~120 and ~185 km, Figure 7a), or (3) the high-velocity lower crust bounded by the top reflection. The seismic images, together with basement samples, support a volcanic basement within the EAB (Booth-Rea et al., 2007, 2018; Duggen et al., 2004, 2008; Gómez de la Peña et al., 2018; Hoernle et al., 1999). All basement samples recovered in the EAB are

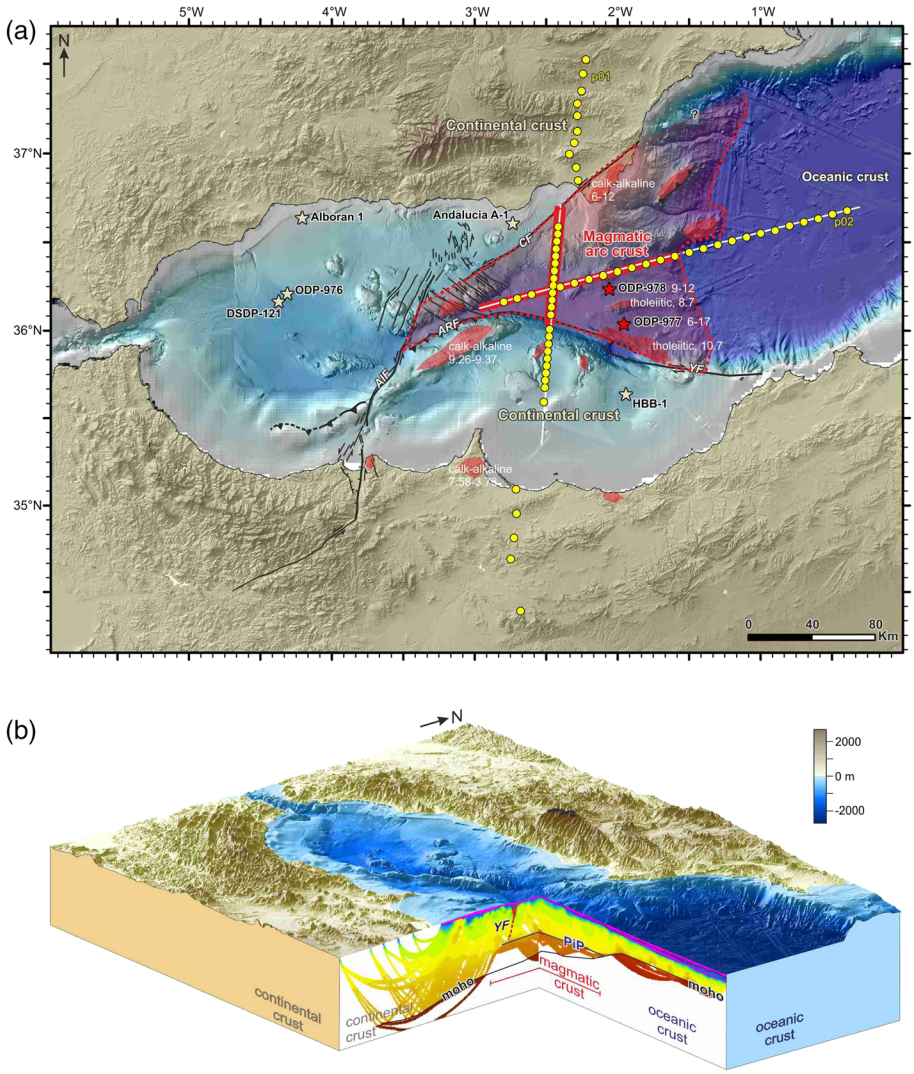

Figure 7. Three-dimensional configuration of the EAB magmatic arc crust. (a) Bathymetric map. Location of basement samples is displayed. The available compositions and ages in Ma of the volcanic samples are shown (Duggen et al., 2004, 2008). Light yellow stars: drilled metamorphic basement. Red stars: drilled volcanic basement. Red polygons: volcanic outcrops. The red rectangles along the p01 and p02 profiles define the area where the magmatic crust is observed in the velocity models. The discontinuous red line encloses the extension of the magmatic arc crust, based on all the observations. AIF, Al-Idrissi Fault; ARF, Alboran Ridge Fault; CF, Carboneras Fault; YF, Yusuf Fault. (b) 3-D view of the crust under the EAB, based on the p01 and p02 sections. Vertical axis is not to scale. YF, Yusuf Fault.

volcanic/magmatic tholeiitic and calc-alkaline rocks (Figure 7a; Duggen et al., 2004, 2005). Thus, we interpreted the high-velocity anomalies observed in the upper crust as volcanic intrusions (Figures 4b and 4c). These rocks are related with an arc to back-arc setting in a subduction context (Duggen et al., 2008).

The layering observed in the lower crust along MCS profiles may be interpreted as magmatic sill-like intrusions (Booth-Rea et al., 2007, 2018). Even though the velocity-lithology correlation depends on the thermal gradient and the comparison between different areas is not direct, similar magmatic intrusions at the base of the crust have been interpreted as mafic/ultramafic deposits in other magmatic arcs (e.g., Tonga arc: Contreras-Reyes et al., 2011; Mariana arc: Calvert et al., 2008; Izu-Bonin arc: Kodaira et al., 2007; Aleutian arc: Shillington et al., 2004), suggesting a similar composition for the EAB lower crust. These mafic/ultramafic deposits are interpreted as the residual of fractionation and partial melting processes (Shillington et al., 2004; Tatsumi et al., 2008). Despite thickness variability, the lower crust velocity is

similar between the central part of the magmatic arc crust and the north and south boundaries (Figure 5d), supporting a homogeneous lower crust composition.

The ~0.25 km/s velocity difference between p01 and p02 profiles (Figure 5h) is also supported by the MCS profiles, where the reflections within the lower crust are stronger and more continuous along W-E transects than in the N-S section (Figure 6). Different velocities between perpendicular profiles across and along the arc have also been reported in the Aleutian arc, where this difference has been attributed to the fore-arc crust effect in the raypaths (Shillington et al., 2004). In the EAB arc, we cannot discard that the continental margins affect the lower crustal velocities along p01 profile. However, as the lower crust layering is also more prominent in the W-E MCS transect than in the N-S (Figure 6), we suggest that the difference in seismic velocity can be related to anisotropy in the lower crust, with the fastest *Vp* parallel to the basin opening direction.

Mature arcs typically have an intermediate composition middle crust, with velocities ~6 km/s, and the absence of these middle-crust velocities indicates a relative mafic composition related to the early stages of arc development (Tatsumi et al., 2008). The velocities in the middle crust of the EAB range between ~6 and 6.6 km/s (Figure 5h). A particular feature of the EAB magmatic arc is the short time period of activity. First evidences of extension in the Alboran Basin are from the Late Oligocene-Early Miocene, represented by onshore dykes (Malaga dykes, Late Oligocene-Early Miocene, Duggen et al., 2004) and the first sediments in the basin (West Alboran Basin, Burdigalian, Comas et al., 1999). Volcanic activity in the basin stopped at ~5–6 Ma, which is in agreement with a Late Miocene cease of the subduction (Iribarren et al., 2007). Thus, the EAB magmatic arc was formed in <20 Ma. The short period of activity, together with the ~6.4 km/s mean velocity in the middle crust, suggest that the EAB never reached a mature stage of evolution.

5.1.3. Continental Crust Under the Pytheas Basin and the North African Margin

In the southern part of the WAS profile (Figure 3a, km 200–360) we do not observe any discontinuity related to the onshore-offshore transition (Figure 3, km ~270; Figure 5e). The crust shows the same characteristics and velocity trend in the southern Alboran Basin (Pytheas Basin) and in Morocco (Figure 5e), with the Moho progressively dipping toward the south and the crust thickening from ~20 to ~28 km (Figure 3a, km 200–360). The velocity structure supports a continental affinity for both regions, the Pytheas basin and the Morocco margin (Figures 5e and 7), which is in agreement with the metamorphic rocks drilled offshore in the HBB-1 well, equivalent to the ones cropping out along the coast of the Eastern Rif (Figure 7a, Azdimousa et al., 2019; Medaouri et al., 2014). Our results are consistent with the velocity structure and Moho depths obtained by Gil et al. (2014) onshore East Morocco. This area shows similar velocity characteristics as the south Iberian margin, although the internal structure is better constrained, especially offshore. The crust can be divided into upper and lower crust, based on velocity differences with velocities increasing from ~5.5 km/s in the upper crust to 6.8 km/s in the lower crust.

In this area, volcanic intrusions are observed and characterized by a high-velocity anomaly in the upper crust and high reflectivity on the MCS profile (Figure 3a, km 220–230; Figure 5e). However, these intrusions show a local character and are mainly bounded by the upper crust (to 8 km depth from the basement top, Figure 5e). Thus, magmatism is not altering the entire crust, which preserves its continental affinity (Figure 5e). Sampled volcanic outcrops in the North African margin support a calk-alkaline composition (Figure 7a, Duggen et al., 2004, 2008), which can be explained by (1) lower degree of partial melting in these areas relative to the central parts of the EAB and/or (2) interaction of the melts with metasomatized mantle or metamorphic crust (Duggen et al., 2008). We hypothesize that these intrusions are related to the magmatic arc crust marginal volcanic activity.

5.2. Implications for Geodynamic Models

Early studies of the Alboran Basin interpreted the basement as thinned continental crust locally affected by volcanism (Comas et al., 1999; Watts et al., 1993). This hypothesis was based on the drilled samples of metamorphic rocks recovered in DSDP Leg 121, ODP Leg 161 Site 976 and the Alboran 1 and Andalucia A-1 commercial wells (Figures 1 and 7a), and a rift-basin type inferred interpretation of seismic images (Watts et al., 1993). However, the metamorphic basement was drilled in the West Alboran Basin and close to the South Iberian coastline and not in the EAB (Figure 7a). Later sampling by dredging of volcanic/magmatic rocks across most of the EAB (Figure 7a; Duggen et al., 2004) supported a wide area affected by volcanism, rather than the isolated intrusions inferred from volcanoclastic sediment recovered in the ODP Leg 161 977 and 978 wells (Comas et al., 1999).

With the improvement of acquisition and processing methods of seismic data and the increased number of basement samples, a better understanding of the crust was achieved. A WSW-ENE MCS profile revealed the internal structure of the EAB crust (ESCI-Alb2, Booth-Rea et al., 2007). The crustal thickness and internal layering observed support its interpretation as magmatic arc crust (Booth-Rea et al., 2007), and not as thinned continental crust. The hypothesis of a magmatic arc flooring the EAB gained support (Booth-Rea et al., 2007, 2018; Duggen et al., 2005, 2008; Gómez de la Peña et al., 2018), although some studies proposed thinned continental crust affected by magmatism (Medaouri et al., 2014). The N-S p01 profile allows (1) to confirm the existence of magmatic arc crust flooring the EAB (Figures 5d and 5h), (2) to constrain the dimensions of this crust identifying its northern and southern boundaries (Figures 4–6 and 7a), and (3) to understand the relation of this magmatic crust with the Iberian and African continental crusts (Figure 7).

The existence of magmatic arc crust flooring the EAB has implications for the Alboran Basin formation models. The convective removal (Dewey et al., 1989; Platt & Vissers, 1989) and the mantle delamination (García-Dueñas et al., 1992; Seber et al., 1996) models will produce an extended continental crust flooring the entire basin, which is supported neither by seismic data nor by the volcanic rocks affinities and distribution. In addition, improved regional tomographic models image clearly an arcuate high-velocity anomaly hanging below the Straits of Gibraltar, which is detached from the surface under the eastern Betics (Chertova et al., 2014; Fichtner & Villaseñor, 2015; Wortel & Spakman, 2000). This anomaly is interpreted as a subducted slab, teared under the eastern Betics, and supports that extension took place in subduction-driven model (Wortel & Spakman, 2000). Thus, all evidences support that pervasive extension and magmatic accretion produced the current magmatic crust flooring the EAB in a subduction setting during the Late Miocene (Faccenna et al., 2004; Spakman & Wortel, 2004) and that the EAB is the magmatic arc of this subduction system.

5.3. Seismogenic Structure

5.3.1. Tectonic Structure

Comparison between the WAS *Vp* model and the MCS image provides the detailed geometry of basins, fault systems, and basement domains. The sedimentary cover is well resolved in the velocity model (Figure 4). Although the *Vp* model does not delineate the basement top in detail, especially in areas with rough geometry (Figure 4b, km 150–160), low-velocity zones are coincident with the main sedimentary depocenters (e.g., Yusuf Basin: Figures 3 and 4 at km ~170; Pytheas Basin: Figures 3 and 4 at km 190–220), while high-velocity anomalies near the surface are in agreement with the location of volcanic intrusions (Figures 3 and 4 at km ~120 and ~185). Within the sedimentary cover, velocities of ~3 km/s are broadly consistent with the Pliocene-Miocene transition (*M* reflection, green dashed line in Figures 4b and 4c). Two sedimentary packages can be defined on the basis of their velocities: a Plio-Quaternary sequence with velocities lower than 3 km/s and a Late Miocene sequence with velocities between 3 and 4.2 km/s. As in the case of the basement top, local variations cannot be fully resolved.

The top of the highly reflective lower crust in MCS images correlates well with the PiP reflection, delineating the top of the high-velocity lower crust in the WAS *Vp* model (Figures 4b and 4c, km 135–180, Figure 6). The location of the *PmP* reflection is also in agreement with the Moho interpreted in the MCS profiles (Figures 4b, 4c, and 6). Small differences in the correlation (<0.5 s TWTT) can be explained by the uncertainty in imaging a 3-D surface across a 2-D transect (Hobbs et al., 2006) or due to crustal anisotropy (Mjelde et al., 1993; Prada et al., 2016; Sallarès et al., 2013). In the westernmost Mediterranean, radial anisotropy has been documented at upper mantle levels (*Pn* anisotropy <0.5 km/s, Díaz et al., 2013).

On the MCS profile, the high reflectivity lower crust terminates abruptly toward the Yusuf Fault to the south (Figures 4c and 7; Gómez de la Peña et al., 2018) and toward the Carboneras Fault to the north (Figures 6a and 7a; Gómez de la Peña et al., 2018). Based on crustal reflectivity patterns, previous studies proposed that major tectonic structures are located mainly offshore along the boundaries between the different crustal domains (Gómez de la Peña et al., 2018; Gràcia et al., 2019). The p01 velocity model indicates that the Yusuf Fault is associated with a relative low-velocity zone at ~170 km, reaching ~10 km depth, which may be indicative of a broad zone accommodating fault damage (Figures 4a and 4b). The crustal-scale tectonic features bounding domains indicate that narrow transition zones between different crustal affinities (~10 km width, Figure 5a, km 80–90 and 190–210) controls focusing of deformation and that crustal structure conditions the current location of the main tectonic features bounding the EAB, namely, the Yusuf

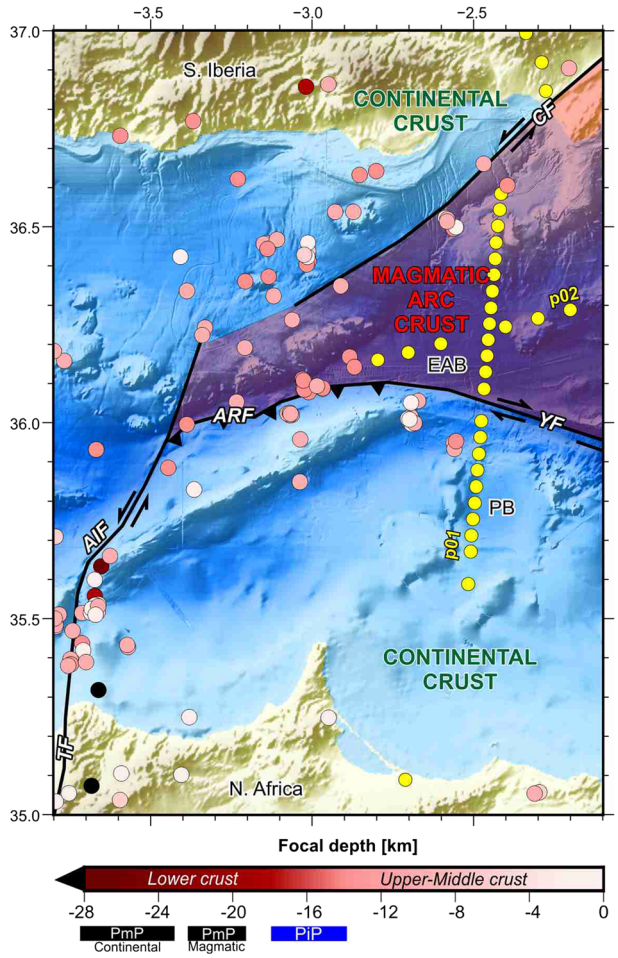

Figure 8. Bathymetric map of the EAB, PB, and their margins (see location in Figure 1a). The dots shown the earthquake location (Grevemeyer et al., 2015) and the color scale shows the nucleation depth. Depths of the lower crust top (PiP) and of the Moho reflections under the magmatic and continental crusts are indicated. The location of the p01 and p02 OBH/S and onshore stations is displayed (yellow dots), as well as the main tectonic structures and the crustal affinities. AIF, Al-Idrissi Fault; ARF, Alboran Ridge Fault; EAB, East Alboran Basin; PB, Pytheas Basin; TF, Trougout Fault; YF, Yusuf Fault.

Fault and the Carboneras Fault (Figures 1 and 7). The reactivation of inherited crustal structures has made that the fault systems are continuous for >100 km possibly since their inception. Their substantial dimensions in continental crust indicate that they might be associated with a significant seismogenic potential at shallow depth.

5.3.2. Implications for Earthquake Nucleation

Previous studies pointed out that seismicity in the area is constrained to crustal depths, being shallower than 20 km in the EAB area (Gràcia et al., 2019; Grevemeyer et al., 2015), but the information on crustal domains was limited. We compare the crustal thickness and tectonic structure interpreted from our WAS velocity model with a database of earthquakes recorded by a temporary OBS network (Figure 8; Grevemeyer et al., 2015), relocated using an offshore-onshore local seismological network and thus with an accuracy that can be compared to the detailed crustal structure in our work. The comparison provides the first modern comparison at regional scale of seismicity distribution, seismic structure, and seismogenic faults distribution (Figure 8). Even though by using this network we only have information of a limited time period, it has two main advantages: a lower uncertainty in the event location and the inclusion of low magnitude events, which cannot be identified at onshore stations. Based on the comparison between the crustal structure resolved by the WAS *Vp* model and the focal depths, two main features are observed: (1) earthquakes are mainly nucleated at upper-middle crust depths and (2) outside of the magmatic arc crust.

All the events recorded at the EAB and its margins are constrained to crustal depths (Figure 8). Moreover, most of the recorded earthquakes occurred at the upper and middle crust, with hypocenters shallower than 15 km depth (pink colored dots at Figure 8). Deeper events occurred close to the Al-Idrissi-Trougout-Nekor fault system (Figure 8: 35.0–35.3°N, −3.5°W) and onshore South Iberia (Figure 8: 36.9°N, −3°W). The Al-Idrissi-Trougout-Nekor fault system is bounding two crustal domains with different thickness (Gil et al., 2014; Gràcia et al., 2019). WAS experiments onshore Morocco support that the Moho is located at >40 km depth western of the Nekor fault system, while it is at ~28 km depth eastern of this fault system (Gil et al., 2014). Although the crust is thinner offshore, this change in crustal thickness is also observed across the Al-Idrissi fault system (Gràcia et al., 2019). This change in crustal configuration could explain the deeper focal depth observed in the proximity of the Al-Idrissi-Trougout-Nekor fault system (Figure 8). In addition, a thickening of the seismogenic layer toward the basin margins due to a lower heat flow in these areas has been already pointed out by Grevemeyer et al. (2015) and can explain the deeper events occurring onshore North Africa and South Iberia (Figure 8).

An interesting observation is that most earthquakes occur outside of the magmatic arc crust, and only a few events close to the magmatic arc crust were recorded (Figure 8). The low seismicity in the magmatic arc crust might be related with a higher thermal gradient in this area, consistent with the magmatic arc crustal affinity and the magmatic intrusions/extrusions found in the EAB.

6. Conclusions

Our WAS velocity model provides a high-resolution *P* wave velocity distribution across the South Iberian margin, the EAB, and the North African continental shelf (Pytheas Basin) and coastal area, sampling the crust and upper mantle.

The continental crust of the South Iberian margin is ~30 km thick and characterized by velocities between 4.5 and 5 km/s in the upper crust and between ~6 and 6.6 km/s in the lower crust. Energy recorded on onshore stations supports a complex internal structure, confirmed by the geology of the area that cannot be fully resolved in our model due to the lack of crossing rays in this section. Mantle velocities are ~7.9 km/s.

The EAB crust is characterized by ~18 km thick crust, well structured into upper (~5.4 km/s), middle (6–6.6 km/s), and lower crust (~7 km/s). The velocity gradient in this area, together with the calk-alkaline to tholeiitic volcanic rock samples and the reflective characteristics of the crust on seismic images, endorse its interpretation as a magmatic arc crust.

The velocity profile shows the extension toward the north of the African continental crust that floored the Pytheas Basin area offshore. This crust is characterized by a thickening from 22 km below the Pytheas Basin to 28 km toward the continent and by velocities ranging from 5.6 to 6.5 km/s in the upper crust to ~6.8 km/s on the lower crust.

Instrumental seismic activity occurs mainly in the upper and middle continental crust. The crustal configuration is not related to the onshore-offshore transition. The major faults in the area are located offshore and seem to be engendered at the boundaries between different crustal domains.

Data Availability Statement

The WESTMED data are archived at PANGAEA repository (https://doi.pangaea.de/10.1594/PANGAEA.921252), GEBCO bathymetry grid (https://doi.org/10.5285/a29c5465-b138-234d-e053-6c86abc040b9), and SRTM bathymetry/topography grid (https://doi.org/10.5067/MEaSUREs/SRTM/SRTMGL1.003).

Acknowledgments

This work is supported by the Cluster of Excellence "The Future Ocean", within the framework of the Excellence Initiative by the Deutsche Forschungsgemeinschaft (DFG) on behalf of the German federal and state governments. Efforts benefitted from funding of the German Science Foundation (DFG Grants GR1964/12-1, RA 925/2-1+2-2, and RE 873/17-1). The TOPOMED cruise was part of the EUROMARGINS and TOPO-EUROPE initiatives of the EUROCORES Programme of the European Science Foundation (ESF). This study benefitted from an EU Marie Skłodowska-Curie Individual Fellowship to L. Gómez de la Peña (H2020-MSCA-IF-2017 796013). The Spanish Science and Innovation Ministry funded C. R. Ranero through the project FRAME CTM2015-71766-R and G. Booth-Rea through the project PID2019-107138RB-I00. This is a contribution of the Barcelona Center for Subsurface Imaging, Grup de Recerca 2017 SGR 1662, Generalitat de Catalunya. The authors thank the reviewers, Dominik Kardell and Robert Allen, and the Associate Editor for their constructive and detailed comments.

References

Azdimousa, A., Jabaloy-Sánchez, A., Münch, P., Martínez-Martínez, J. M., Booth-Rea, G., Vázquez-Vílchez, M., et al. (2019). Structure and exhumation of the Cap des Trois Fourches basement rocks (Eastern Rif, Morocco). *Journal of African Earth Sciences*, *150*, 657–672. https://doi.org/10.1016/J.JAFREARSCI.2018.09.018

Ballesteros, M., Rivera, J., Muñoz, A., Muñoz-martín, A., Acosta, J., Carbó, A., & Uchupi, E. (2008). Alboran Basin, southern Spain—Part II: Neogene tectonic implications for the orogenic float model. *Marine and Petroleum Geology*, *25*(1), 75–101. https://doi.org/10.1016/j.marpetgeo.2007.05.004

Banda, E., Gallart, J., García-Dueñas, V., Dañobeitia, J. J., & Makris, J. (1993). Lateral variation of the crust in the Iberian peninsula: New evidence from the Betic Cordillera. *Tectonophysics*, *221*(1), 53–66. https://doi.org/10.1016/0040-1951(93)90027-H

Bezada, M. J., Humphreys, E. D., Toomey, D. R., Harnafi, M., Dávila, J. M., & Gallart, J. (2013). Evidence for slab rollback in westernmost Mediterranean from improved upper mantle imaging. *Earth and Planetary Science Letters*, *368*, 51–60. https://doi.org/10.1016/j.epsl.2013.02.024

Blanco, M. J., & Spakman, W. (1993). The P-wave velocity structure of the mantle below the Iberian Peninsula: Evidence for subducted lithosphere below southern Spain. *Tectonophysics*, *221*(1), 13–34. https://doi.org/10.1016/0040-1951(93)90025-F

Bonnin, M., Nolet, G., Villaseñor, A., Gallart, J., & Thomas, C. (2014). Multiple-frequency tomography of the upper mantle beneath the African/Iberian collision zone. *Geophysical Journal International*, *198*(3), 1458–1473. https://doi.org/10.1093/gji/ggu214

Booth-Rea, G., Martínez-Martínez, J. M., & Giaconia, F. (2015). Continental subduction, intracrustal shortening, and coeval upper-crustal extension: P-T evolution of subducted south Iberian paleomargin metapelites (Betics, SE Spain). *Tectonophysics*, *663*, 122–139. https://doi.org/10.1016/j.tecto.2015.08.036

Booth-Rea, G., Ranero, C. R., & Grevemeyer, I. (2018). The Alboran volcanic-arc modulated the Messinian faunal exchange and salinity crisis. *Scientific Reports*, *8*(1), 1–14. https://doi.org/10.1038/s41598-018-31307-7

Booth-Rea, G., Ranero, C. R., Martínez-Martínez, J. M., & Grevemeyer, I. (2007). Crustal types and Tertiary tectonic evolution of the Alborán sea, western Mediterranean. *Geochemistry, Geophysics, Geosystems*, *8*, Q10005. https://doi.org/10.1029/2007GC001639

Calvert, A. J. (2011). The seismic structure of island arc crust. In D. Brown, & P. D. Ryan (Eds.), *Arc-continent collision* (pp. 87–119). Berlin Heidelberg: Springer-Verlat. https://doi.org/10.1007/978-3-540-88558-0_4

Calvert, A. J., Klemperer, S. L., Takahashi, N., & Kerr, B. C. (2008). Three-dimensional crustal structure of the Mariana island arc from seismic tomography. *Journal of Geophysical Research*, *113*, B01406. https://doi.org/10.1029/2007JB004939

Chertova, M. V., Spakman, W., Geenen, T., van den Berg, A. P., & van Hinsbergen, D. J. J. (2014). Underpinning tectonic reconstruction of the western Mediterranean region with dynamic slab evolution from 3-D numerical modeling. *Journal of Geophysical Research: Solid Earth*, *119*, 1119–1144. https://doi.org/10.1002/2013JB010500

Christensen, N. I., & Mooney, W. D. (1995). Seismic velocity structure and composition of the continental crust: A global view. *Journal of Geophysical Research*, *100*(B6), 9761–9788. https://doi.org/10.1029/95JB00259

Christeson, G. L., Goff, J. A., & Reece, R. S. (2019). Synthesis of oceanic crustal structure from two-dimensional seismic profiles. *Reviews of Geophysics*, *57*, 504–529. https://doi.org/10.1029/2019RG000641

Comas, M. C., Platt, J. P., Soto, J. I., & Watts, A. B. (1999). 44. The origin and tectonic history of the Alboran Basin: Insights from leg 161 results. *Proceeding of the Ocean Drilling Program, Scientific Results*, *161*, 555–580.

Comas, M. C., & Soto, J. I. (1999). Brittle deformation in the metamorphic basement at Site 976: Implications for middle Miocene extensional tectonics in the Western Alboran Basin. *Proceedings of the Ocean Drilling Program, 161 Scientific Results*, *161*, 331–344. https://doi.org/10.2973/odp.proc.sr.161.226.1999

Contreras-Reyes, E. C., Grevemeyer, I., Watts, A. B., Flueh, E. R., Peirce, C., Moeller, S., & Papenberg, C. (2011). Deep seismic structure of the Tonga subduction zone: Implications for mantle hydration, tectonic erosion, and arc magmatism. *Journal of Geophysical Research*, *116*, B10103. https://doi.org/10.1029/2011JB008434

Crespo-Blanc, A., & Frizon de Lamotte, D. F. (2006). Structural evolution of the external zones derived from the Flysch trough and the South Iberian and Maghrebian paleomargins around the Gibraltar arc: A comparative study. *Bulletin de la Societe Geologique de France*, *177*(5), 267–282. https://doi.org/10.2113/gssgfbull.177.5.267

Dewey, J. F., Helman, M. L., Knott, S. D., Turco, E., & Hutton, D. H. W. (1989). Kinematics of the western Mediterranean. *Geological Society, London, Special Publications*, *45*(1), 265–283. https://doi.org/10.1144/GSL.SP.1989.045.01.15

Díaz, J., Gallart, J., & Carbonell, R. (2016). Moho topography beneath the Iberian-Western Mediterranean region mapped from controlled-source and natural seismicity surveys. *Tectonophysics*, *692*, 74–85. https://doi.org/10.1016/j.tecto.2016.08.023

Díaz, J., Gil, A., & Gallart, J. (2013). Uppermost mantle seismic velocity and anisotropy in the Euro-Mediterranean region from Pn and Sn tomography. *Geophysical Journal International*, *192*(1), 310–325. https://doi.org/10.1093/gji/ggs016

Duggen, S., Hoernle, K., Klügel, A., Geldmacher, J., Thirlwall, M., Hauff, F., et al. (2008). Geochemical zonation of the Miocene Alborán Basin volcanism (westernmost Mediterranean): Geodynamic implications. *Contributions to Mineralogy and Petrology*, *156*(5), 577–593. https://doi.org/10.1007/s00410-008-0302-4

Duggen, S., Hoernle, K., van den Bogaard, P., & Garbe-Schönberg, D. (2005). Post-collisional transition from subduction-to intraplate-type magmatism in the westernmost Mediterranean: Evidence for continental-edge delamination of subcontinental lithosphere. *Journal of Petrology*, *46*(6), 1155–1201. https://doi.org/10.1093/petrology/egi013

Duggen, S., Hoernle, K., van den Bogaard, P., & Harris, C. (2004). Magmatic evolution of the Alboran region: The role of subduction in forming the western Mediterranean and causing the Messinian Salinity Crisis. *Earth and Planetary Science Letters*, *218*(1–2), 91–108. https://doi.org/10.1016/S0012-821X(03)00632-0

Faccenna, C., Becker, T. W., Auer, L., Billi, A., Boschi, L., Brun, J. P., et al. (2014). Mantle dynamics in the Mediterranean. *Reviews of Geophysics*, *52*, 283–332. https://doi.org/10.1002/2013RG000444

Faccenna, C., Piromallo, C., Crespo-Blanc, A., Jolivet, L., & Rossetti, F. (2004). Lateral slab deformation and the origin of the western Mediterranean arcs. *Tectonics*, *23*, TC1012. https://doi.org/10.1029/2002TC001488

Fichtner, A., & Villaseñor, A. (2015). Crust and upper mantle of the western Mediterranean—Constraints from full-waveform inversion. *Earth and Planetary Science Letters*, *428*, 52–62. https://doi.org/10.1016/j.epsl.2015.07.038

Gallart, J., Díaz, J., Vidal, N., & Dañobeitia, J. J. (1995). The base of the crust at the Betics-Alborán Sea transition: Evidence for and abrupt structural variation from wide-angle ESCI data. *Revista de la Sociedad Geológica de España*, *8*(4), 519–527.

Garcia-Castellanos, D., & Villaseñor, A. (2011). Messinian salinity crisis regulated by competing tectonics and erosion at the Gibraltar arc. *Nature*, *480*(7377), 359–363. https://doi.org/10.1038/nature10651

García-Dueñas, V., Balanyá, J. C., & Martínez-Martínez, J. M. (1992). Miocene extensional detachments in the outcropping basement of the northern Alboran Basin (Betics) and their tectonic implications. *Geo-Marine Letters*, *12*(2–3), 88–95. https://doi.org/10.1007/BF02084917

Giaconia, F., Booth-Rea, G., Ranero, C. R., Gràcia, E., Bartolome, R., Calahorrano, A., et al. (2015). Compressional tectonic inversion of the Algero-Balearic basin: Latemost Miocene to present oblique convergence at the Palomares margin (Western Mediterranean). *Tectonics*, *34*, 1516–1543. https://doi.org/10.1002/2015TC003861

Gil, A., Gallart, J., Diaz, J., Carbonell, R., Torne, M., Levander, A., & Harnafi, M. (2014). Crustal structure beneath the Rif Cordillera, North Morocco, from the RIFSIS wide-angle reflection seismic experiment. *Geochemistry, Geophysics, Geosystems*, *15*, 4712–4733. https://doi.org/10.1002/2014GC005485

Gómez de la Peña, L., Gràcia, E., Muñoz, A., Acosta, J., Gómez-Ballesteros, M., Ranero, C., & Uchupi, E. (2016). Geomorphology and Neogene tectonic evolution of the Palomares continental margin (Western Mediterranean). *Tectonophysics*, *689*, 25–39. https://doi.org/10.1016/j.tecto.2016.03.009

Gómez de la Peña, L., Ranero, C. R., & Gràcia, E. (2018). The crustal domains of the Alboran Basin (western Mediterranean). *Tectonics*, *37*, 3352–3377. https://doi.org/10.1029/2017TC004946

Gràcia, E., Bartolome, R., Lo Iacono, C., Moreno, X., Stich, D., Martínez-Diaz, J. J., et al. (2012). Acoustic and seismic imaging of the Adra Fault (NE Alboran Sea): In search of the source of the 1910 Adra earthquake. *Natural Hazards and Earth System Sciences*, *12*(11), 3255–3267. https://doi.org/10.5194/nhess-12-3255-2012

Gràcia, E., Dañobeitia, J., Vergés, J., & Bartolome, R. (2003). Crustal architecture & tectonic evolution of the Gulf of Cadiz (SW Iberian Margin) at the convergence of the Eurasian & African plates. *Tectonics*, *22*(4), 1033. https://doi.org/10.1029/2001TC901045

Gràcia, E., Grevemeyer, I., Bartolomé, R., Perea, H., Martínez-Loriente, S., Gómez de la Peña, L., et al. (2019). Earthquake crisis unveils the growth of an incipient continental fault system. *Nature Communications*, *10*(1), 1–11. https://doi.org/10.1038/s41467-019-11064-5

Gràcia, E., Pallàs, R., Soto, J. I., Comas, M., Moreno, X., Masana, E., et al. (2006). Active faulting offshore SE Spain (Alboran Sea): Implications for earthquake hazard assessment in the Southern Iberian Margin. *Earth and Planetary Science Letters*, *241*(3–4), 734–749. https://doi.org/10.1016/j.epsl.2005.11.009

Grevemeyer, I., Gràcia, E., Villaseñor, A., Leuchters, W., & Watts, A. B. (2015). Seismicity and active tectonics in the Alboran Sea, Western Mediterranean: Constraints from an offshore-onshore seismological network and swath bathymetry data. *Journal of Geophysical Research: Solid Earth*, *121*, 767–787. https://doi.org/10.1002/2015JB012352

Grevemeyer, I., Ranero, C. R., & Ivandic, M. (2018). Structure of oceanic crust and serpentinization at subduction trenches. *Geosphere*, *14*(2), 395–418. https://doi.org/10.1130/GES01537.1

Hobbs, R. W., Drummond, B. J., & Goleby, B. R. (2006). The effects of three-dimensional structure on two-dimensional images of crustal seismic sections and on the interpretation of shear zone morphology. *Geophysical Journal International*, *164*(3), 490–500. https://doi.org/10.1111/j.1365-246X.2006.02814.x

Hoernle, K., van den Bogaard, P., Duggen, S., Mocek, B., & Garbe-Schönberg, D. (1999). Evidence for Miocene subduction beneath the Alboran Sea: $^{40}Ar/^{39}Ar$ dating and geochemistry of volcanic rocks from Holes 977A and 978A. *Proceedings of the Ocean Drilling Program*. https://doi.org/10.2973/odp.proc.sr.161.264.1999

Iribarren, L., Vergés, J., Camurri, F., Fullea, J., & Fernàndez, M. (2007). The structure of the Atlantic-Mediterranean transition zone from the Alboran Sea to the Horseshoe Abyssal Plain (Iberia-Africa plate boundary). *Marine Geology*, *243*(1–4), 97–119. https://doi.org/10.1016/j.margeo.2007.05.011

Jurado, M. J., & Comas, M. C. (1992). Well log interpretation and seismic character of the Cenozoic sequence in the northern Alboran Sea. *Geo-Marine Letters*, *12*(2-3), 129–136. https://doi.org/10.1007/BF02084923

Kodaira, S., Sato, T., Takahashi, N., Ito, A., Tamura, Y., Tatsumi, Y., & Kaneda, Y. (2007). Seismological evidence for variable growth of crust along the Izu intraoceanic arc. *Journal of Geophysical Research*, *112*, B05104. https://doi.org/10.1029/2006JB004593

Korenaga, J., Holbroook, K., Kelemen, D., Detrick, R. S., Larsen, H.-. C., Hopper, J. R., & Dahl-Jensen, T. (2000). Crustal structure of the southeast Greenland margin from joint refraction and reflection seismic tomography. *Journal of Geophysical Research*, *105*(B9), 21,591–21,614. https://doi.org/10.1029/2000JB900188

Luján, M., Crespo-Blanc, A., & Balanyá, J. C. (2006). The Flysch Trough thrust imbricate (Betic Cordillera): A key element of the Gibraltar Arc orogenic wedge. *Tectonics*, *25*, TC6001. https://doi.org/10.1029/2005TC001910

Mancilla, F. d. L., Booth-Rea, G., Stich, D., Pérez-Peña, J. V., Morales, J., Azañón, J. M., et al. (2015). Slab rupture and delamination under the Betics and Rif constrained from receiver functions. *Tectonophysics*, *663*, 225–237. https://doi.org/10.1016/j.tecto.2015.06.028

Mancilla, F. d. L., & Diaz, J. (2015). High resolution Moho topography map beneath Iberia and Northern Morocco from receiver function analysis. *Tectonophysics*, *663*, 203–211. https://doi.org/10.1016/j.tecto.2015.06.017

Maramai, A., Brizuela, B., & Graziani, L. (2014). The Euro-Mediterranean Tsunami Catalogue. *Annals of Geophysics*, *57*(4), S0435. https://doi.org/10.4401/ag-6437

Marchesi, C., Garrido, C. J., Bosch, D., Bodinier, J. L., Hidas, K., Padrón-Navarta, J. A., & Gervilla, F. (2012). A late Oligocene suprasubduction setting in the westernmost Mediterranean revealed by intrusive pyroxenite dikes in the Ronda Peridotite (southern Spain). *The Journal of Geology*, *120*(2), 237–247. https://doi.org/10.1086/663875

Martínez-García, P., Comas, M., Soto, J. I., Lonergan, L., & Watts, A. B. (2013). Strike-slip tectonics and basin inversion in the Western Mediterranean: The post-Messinian evolution of the Alboran Sea. *Basin Research*, *25*(4), 361–387. https://doi.org/10.1111/bre.12005

McClusky, S., Reilinger, R., Mahmoud, S., Ben Sari, D., & Tealeb, A. (2003). GPS contraints on Africa and Arabi plate motions. *Geophysical Journal International*, *155*(1), 126–138. https://doi.org/10.1046/j.1365-246X.2003.02023.x

Medaouri, M., Déverchère, J., Graindorge, D., Bracene, R., Badji, R., Ouabadi, A., et al. (2014). The transition from Alboran to Algerian basins (Western Mediterranean Sea): Chronostratigraphy, deep crustal structure and tectonic evolution at the rear of a narrow slab rollback system. *Journal of Geodynamics*, *77*, 186–205. https://doi.org/10.1016/j.jog.2014.01.003

Michard, A., de Lamotte, D. F., Saddiqi, O., & Chalouan, A. (2008). Chapter 1: An outline of the geology of Morocco. In *Continental evolution: The geology of Morocco*, *Lecture Notes in Earth Sciences* (Vol. 116). Berlin, Heidelberg: Springer-Verlag. https://doi.org/10.1007/978-3-540-77076-3_5

Mjelde, R., Sellevoll, M. A., Shimamura, H., Iwasaki, T., & Kanazawa, T. (1993). Crustal structure beneath Lofoten, N. Norway, from vertical incidence and wide-angle seismic data. *Geophysical Jounal of Astronomical Society*, *114*(1), 116–126. https://doi.org/10.1111/j.1365-246X.1993.tb01471.x

Palano, M., González, P. J., & Fernández, J. (2015). The diffuse plate boundary of Nubia and Iberia in the Western Mediterranean: Crustal deformation evidence for viscous coupling and fragmented lithosphere. *Earth and Planetary Science Letters*, *430*, 439–447. https://doi.org/10.1016/j.epsl.2015.08.040

Palomeras, I., Villaseñor, A., Thurner, S., Levander, A., Gallart, J., & Harnafi, M. (2017). Lithospheric structure of Iberia and Morocco using finite-frequency Rayleigh wave tomogrphy from earthquakes and seismic ambient noise. *Geochemistry, Geophysics, Geosystems*, *18*, 1824–1840. https://doi.org/10.1002/2016GC006657

Peláez, J. A., Chourak, M., Tadili, B. A., Aït Brahim, L., Hamdache, M., López Casado, C., & Martínez Solares, J. M. (2007). A catalog of main Moroccan earthquakes from 1045 to 2005. *Seismological Research Letters*, *78*(6), 614–621. https://doi.org/10.1785/gssrl.78.6.614

Perea, H., Gràcia, E., Alfaro, P., Bartolomé, R., Lo Iacono, C., Moreno, X., & Masana, E. (2012). Quaternary active tectonic structures in the offshore Bajo Segura basin (SE Iberian Peninsula - Mediterranean Sea). *Natural Hazards and Earth System Sciences*, *12*(10), 3151–3168. https://doi.org/10.5194/nhess-12-3151-2012

Platt, J. P., Behr, W. M., Johanesen, K., & Williams, J. R. (2013). The Betic-Rif arc and its Orogenic hinterland: A review. *Annual Review of Earth and Planetary Sciences*, *41*(1), 313–357. https://doi.org/10.1146/annurev-earth-050212-123951

Platt, J. P., Kelley, S. P., Carter, A., & Orozco, M. (2005). Timing of tectonic events in the Alpujárride Complex, Betic Cordillera, southern Spain. *Journal of the Geological Society of London*, *162*(3), 451–462. https://doi.org/10.1144/0016-764903-039

Platt, J. P., & Vissers, R. L. M. (1989). Extensional collapse of thickened continental lithosphere: A working hypothesis for the Alboran Sea and Gibraltar Arc. *Geology*, *17*(6), 540–543. https://doi.org/10.1130/0091-7613(1989)017<0540:ECOTCL>2.3.CO;2

Prada, M., Sallares, V., Ranero, C. R., Vendrell, M. G., Grevemeyer, I., Zitellini, N., & de Franco, R. (2016). Spatial variations of magmatic crustal accretion during the opening of the Tyrrhenian back-arc from wide-angle seismic velocity models and seismic reflection images. *Basin Research*, *30*, 124–141. https://doi.org/10.1111/bre.12211

Rovere, M., Ranero, C. R., Sartori, R., Torelli, L., & Zitellini, N. (2004). Seismic images and magnetic signature of the Late Jurassic to Early Cretaceous Africa-Eurasia plate boundary off SW Iberia. *Geophysical Journal International*, *158*(2), 554–568. https://doi.org/10.1111/j.1365-246X.2004.02339.x

Royden, L., & Faccenna, C. (2018). Subduction orogeny and the Late Cenozoic evolution of the Mediterranean Arcs. *Annual Review of Earth and Planetary Sciences*, *46*(1), 261–289. https://doi.org/10.1146/annurev-earth-060115-012419

Royden, L. H. (1993). Evolution of retreating subduction boundaries formed during continental collision. *Tectonics*, *12*(3), 629–638. https://doi.org/10.1029/92TC02641

Sallarès, V., Meléndez, A., Prada, M., Ranero, C. R., Mcintosh, K., & Grevemeyer, I. (2013). Overriding plate structure of the Nicaragua convergent margin: Relationship to the seismogenic zone of the 1992 tsunami earthquake. *Geochemistry, Geophysics, Geosystems*, *14*, 3436–3461. https://doi.org/10.1002/ggge.20214

Sanz De Galdeano, C. (1990). Geologic evolution of the Betic Cordilleras in the Western Mediterranean, Miocene to the present. *Tectonophysics*, *172*(1–2), 107–119. https://doi.org/10.1016/0040-1951(90)90062-D

Seber, D., Barazangi, M., Ibenbrahim, A., & Demnati, A. (1996). Geophysical evidence for lithospheric delamination beneath the Alboran Sea and Rif-Betic mountains. *Nature*, *379*(6568), 785–790. https://doi.org/10.1038/379785a0

Shillington, D. J., Holbrook, W. S., Kelemen, P. B., & Hornbach, M. J. (2004). Composition and structure of the central Aleutian island arc from arc-parallel wide-angle seismic data. *Geochemistry, Geophysics, Geosystems*, *5*, Q10006. https://doi.org/10.1029/2004GC000715

Spakman, W., Chertova, M. V., Van Den Berg, A., & Van Hinsbergen, D. J. J. (2018). Puzzling features of western Mediterranean tectonics explained by slab dragging. *Nature Geoscience*, *11*(3), 211–216. https://doi.org/10.1038/s41561-018-0066-z

Spakman, W., & Wortel, R. (2004). Chapter 2: A tomographic view on western Mediterranean geodynamics. In *The TRANSMED atlas, the Mediterranean region from crust to mantle* (pp. 31–52). Berlin, Heidelberg: Springer-Verlag. https://doi.org/10.1007/978-3-642-18919-7_2

Stich, D., Serpelloni, E., de Lis Mancilla, F., & Morales, J. (2006). Kinematics of the Iberia-Maghreb plate contact from seismic moment tensors and GPS observations. *Tectonophysics*, *426*(3–4), 295–317. https://doi.org/10.1016/j.tecto.2006.08.004

Tatsumi, Y., Shukuno, H., Tani, K., Takahashi, N., Kodaira, S., & Kogiso, T. (2008). Structure and growth of the Izu-Bonin-Mariana arc crust: 2. Role of crust-mantle transformation and the transparent Moho in arc crust evolution. *Journal of Geophysical Research*, *113*, B02203. https://doi.org/10.1029/2007JB005121

The Working Group for Deep Seismic Sounding in the Alboran Sea 1974 (1978). Crustal seismic profiles in the Alboran Sea—Preliminary results. *Pure and Applied Geophysics*, *116*(1), 167–180. https://doi.org/10.1007/BF00878991

Torres-Roldán, R. L., Poli, G., & Peccerillo, A. (1986). An early Miocene arc-tholeitic magmatic dyke event from the Alboran sea: Evidence for precollision subduction and back-arc crustal extension in the westernmost Mediterranean. *Geologische Rundschau*, *75*(1), 219–234. https://doi.org/10.1007/BF01770190

Van Hinsbergen, D. J. J., Vissers, R. L. M., & Spakman, W. (2014). Origin and consequences of western Mediterranean subduction, rollback, and slab segmentation. *Tectonics*, *33*, 393–419. https://doi.org/10.1002/2013TC003349

Villaseñor, A., Chevrot, S., Harnafi, M., Gallart, J., Pazos, A., Serrano, I., et al. (2015). Subduction and volcanism in the Iberia-North Africa collision zone from tomographic images of the upper mantle. *Tectonophysics*, *663*, 238–249. https://doi.org/10.1016/j.tecto.2015.08.042

Watts, A. B., Platt, J. P., & Buhl, P. (1993). Tectonic evolution of the Alboran Sea basin. *Basin Research*, *5*(3), 153–177. https://doi.org/10.1111/j.1365-2117.1993.tb00063.x

White, R. S., McKenzie, D., & O'Nions, R. K. (1992). Oceanic crustal thickness from seismic measurements and rare earth element inversions. *Journal of Geophysical Research*, *97*(B13), 19,683–19,715. https://doi.org/10.1029/92JB01749

Wortel, M. J., & Spakman, W. (2000). Subduction and slab detachment in the Mediterranean-Carpathian region. *Science*, *290*(5498), 1910–1917. https://doi.org/10.1126/science.290.5498.1910

Zitellini, N., Gràcia, E., Matias, L., Terrinha, P., Abreu, M. A., De Alteriis, G., et al. (2009). The quest for the Africa-Eurasia plate boundary west of the Strait of Gibraltar. *Earth and Planetary Science Letters*, *280*(1–4), 13–50. https://doi.org/10.1016/j.epsl.2008.12.005